Characterising Fickian Diffusion On the Surface of a Sphere

Owen Orrick[1], Minjun Yang[1], Christopher Batchelor-McAuley[1], Richard G. Compton[1*]

[1] Physical and Theoretical Chemistry Laboratory, Department of Chemistry, University of Oxford, South Parks Road, Oxford OX1 3QZ, Great Britain

* corresponding author email: Richard.Compton@chem.ox.ac.uk

Abstract

Single-entity electrochemical analysis involving Fickian charge diffusion over the surface of a (truncated) sphere is explored via numerical simulation, mimicking the case where an insulating particle covered with an electroactive adsorbed layer impinges on an electrode. The ever-changing shape of the flux-time transient as the diffusion regimes change over the surface of the sphere from the point of charge injection are characterised with the use of the recently introduced diffusion indicator, α, [Haonan *et. al., J. Electroanal. Chem.* 855, 113602]. The indicator is shown to illuminate, with clarity, the change of diffusion from divergent near the point of injection through linear at the sphere circumference to convergent before being limited by the thin-layer effect as the surface of the sphere is fully oxidised or reduced. Truncated spheres are also examined and characterised along with diffusion under model 'thin layer' conditions.

Keywords: Electrochemistry, nano-impacts, thin layer diffusion, diffusion indicator, numerical simulation

1. Introduction

The area of single entity electrochemistry, with its origins in the polarographic work of Heyrovsky[1-3] and in characterising particles for photography at Kodak[4-5], has evolved rapidly over the last decade[6-10] claiming notable successes in the characterisation of single nanoparticles, in catalysis[11-13], in detecting bacteria[14-15], viruses[16], and in studying the fundamental kinetics of enzyme chemistry[17-18]. One as yet relatively unexplored area, although of high potential use for example in developing agents for environmental clean-up, is the study of adsorption on the surface of individual particles. Thus adsorption onto the surface of conductive single graphene nano-platelets was characterised via nano-impacts by Chen[19] who showed the existence of concentration driven phase changes, notably flat to vertical transitions, by considering the charge passed in a single particle-electrode collision. Adsorption of catechol on non-conductive particles of alumina (Al_2O_3) was demonstrated and quantified in nano-impacts experiments, by Lin.[20-21] In Lin's work, the current – time 'spike' accompanying the particle-electrode collision showed via the total charge passed, that the adsorption was monolayer whilst the transient shape was used to infer that with the impacted electrode held at a suitable over-potential the charge injection was controlled by charge hopping[22] between adsorbed catechol molecules corresponding to two-dimensional surface diffusion necessitated by the insulating character of the bulk particle.

In the present paper we explore the two-dimensional Fickian diffusion of charge on the surface of a sphere and of truncated spheres injected from either a near point source or from the circumference of truncation in the latter case. In particular the specfic challenges of simulating the injection from a single point in this geometry are

addressed and resolved. Further to explain the shape of the flux, j, versus time, t, profiles for charge injection so as to fully oxidise or reduce an adsorbed layer of electroactive molecules we deploy the recently introduced[23] 'diffusion indicator', α, which is defined by

$$\alpha = 2\frac{d(log(J))}{d(log(T))} + 1 \qquad \textit{Equation 1}$$

where J and T is the dimensionless equivalent of flux (j) and time (t), respectively. The conversion between dimensional and dimensionless parameters are discussed in more detailed in the Theory section. Note that the values of α is the same regardless of which form (dimensional or dimensionless) of the flux and time are used.

This diffusion indicator, α, has been used to characterise diffusion in a variety of simple electrode geometries. Note in particular that for linear diffusion into a semi-infinite space the flux-time relationship is given by the Cottrell equation[24]

$$j = \frac{\sqrt{D}c^*}{\sqrt{\pi t}} \qquad \textit{Equation 2}$$

so that α = 0. In contrast for steady-state diffusion such as characterises all but the shortest time responses of microelectrodes such as micro-discs or micro-hemispheres, then since j is invariant with t, α = 1. The diffusion indicator has been used to explore the chrono-amperometric response of micro-cylindrical electrodes[23, 25] where the existence of mixed macro- and micro-dimensions lead to a so-called quasi-steady-state response in which the long-time flux slowly decays with time rather than becoming exactly constant as is seen at, for example, a micro-disc electrode. The diffusion indicator illuminated the response of different zones on the electrode in the case of a cylindrical electrode in which both the sides and the end (top) were active but with different current-time responses.[23] In the present study the indicator is used

to quantify the ever-changing character of the j/t behaviour associated with charge diffusion on the surface of a (truncated) sphere ranging from near linear at the point of injection and again at the diameter of the sphere whilst passing through divergent and then convergent space, as viewed by the apparent diffusion of the charge in the surface layer, before being limited by thin layer effect as the adsorbed layer is fully electrolysed.

2. Theory

The theoretical model involving charge diffusion over the surface of a sphere is first described physically, before, second, the mathematical formulations and the boundary conditions are outlined.

Figure 1 depicts the two-dimensional Fickian charge diffusion over a) a perfect sphere and b) a hemisphere located on a plate from which charge is injected in both cases. Initially, a uniform adsorbed layer of species A is present on the surface with a coverage Γ_A^* (mol m^{-2}). At some time, t =0, species A (ads) is oxidised to form species B (ads), via charge injection into the plate. B is adsorbed and remains on the sphere surface.

$$A(ads) - e^- \rightarrow B(ads) \qquad \textit{Equation 3}$$

The build up of B local to the point of charge injection and the corresponding depletion of A allows for charge to hop between A and B molecules which serves to diffuse the formation of B and depletion of A around the sphere, provided the average separation of A and B species is consistent with electrode tunnelling. Formally this is equivalent to Fickian diffusion under a concentration gradient. The depletion of A (ads) at the particle-electrode boundary concomitantly leads to a coverage gradient and two-dimensional diffusion over the surface of the sphere. Note, the movement of charge is described here simply as pure Fickian diffusion rather than partly via migration. This is not unrealistic as the hopping of electrons between adjacent and available sites are typically coupled with ion motion, through the presence of inert electrolyte in the solution-phase resulting in an 'effective' diffusion coefficient measurable experimentally.[22, 26-27] Since A and B are assumed immobile and the diffusion is via A+B –> B + A (charge hopping) it necessarily follows that $D_A = D_B = D$. The electron-

hopping mechanism is described in more detail elsewhere by Amatore *et al.*[27] The sphere supporting the layer of A and B is electrochemically inert and is assumed stationary with a constant contact angle, $\theta_{contact}$, during the timescale of the simulation (see Figure 1). In the long-time limit, the depletion layer extends over the entirety of the sphere and A(ads) is fully depleted over the surface of the sphere. The next section outlines the above-described model mathematically.

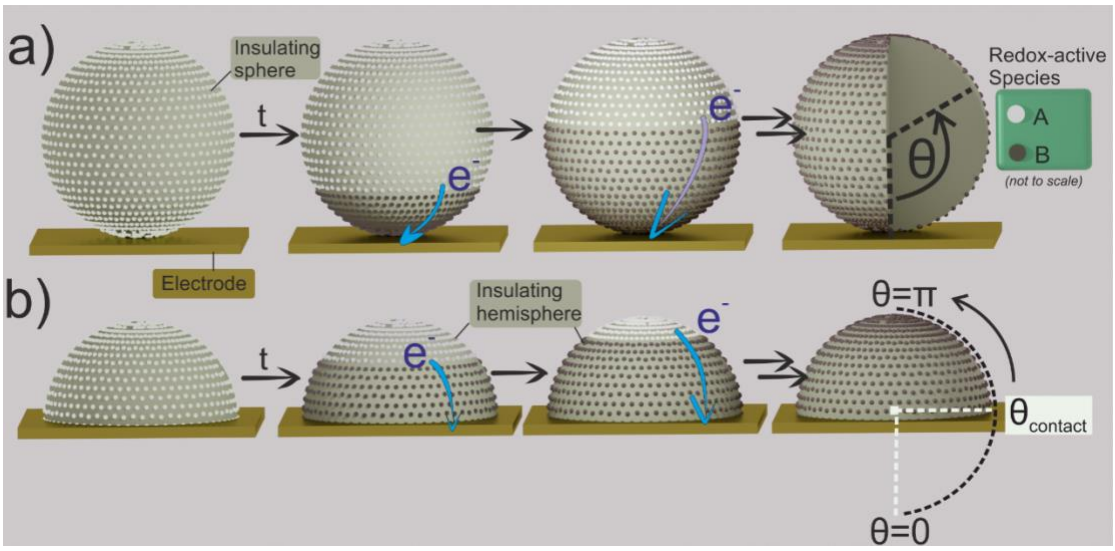

Figure 1. A schematic diagram depicting the two-dimensional charge diffusion over an insulating a) perfect sphere and b) hemisphere. Species A is electrochemically active and initially present as a layer adsorbed on the surface. From t > 0, a sufficient over-potential is applied at the electrode to fully drive the oxidation of A(ads) to form B(ads). Diffusion of charge around the surface of the sphere allows A(ads) to be consumed across the surface until full depletion in the long-time limit.

2.1 Mathematical model

The contact area between the sphere and the electrode is defined by the contact angle, $\theta_{contact}$, from $\theta = 0$ to the edge of the (truncated) sphere-electrode contact, shown in Figure 1. The angle θ has units of radians and may take any value between zero and π:

$$0 < \theta_{contact} < \pi \qquad \textit{Equation 4}$$

For a full sphere in contact with an electrode the contact angle is close to zero, whereas that of a hemisphere is equal to $\pi/2$. The flux at the particle-electrode

interface, j (mol m^{-1} s^{-1}), is defined by the rate of consumption A(ads) or the rate of formation of B(ads) per unit arc length

$$j = -\frac{D}{r_e}\left(\frac{\partial \Gamma_A}{\partial \theta}\right)_{\theta_{contact}} = \frac{D}{r_e}\left(\frac{\partial \Gamma_B}{\partial \theta}\right)_{\theta_{contact}} \qquad \textit{Equation 5}$$

where r_e is the radius of the sphere and D is the 'apparent' diffusion coefficient for species A and B, respectively. Alternatively, due to mass conservation, the interfacial flux j, or the rate of consumption, can be calculated via the sum of the rate of change of A(ads) over the surface of the sphere with time:

$$j = r_e \int_{\theta_{contact}}^{\pi} \frac{\partial \Gamma_A}{\partial t} d\theta \qquad \textit{Equation 6}$$

The flux j can be expressed in terms of electrical current, I (A)

$$I = -FCj \qquad \textit{Equation 7}$$

where F is the Faraday constant (96485.3 C mol^{-1}), C is the circumference (m) of the particle-electrode contact $(2\pi sin(\theta) r_e)$. In the presence of a full supporting electrolyte and in the absence of migration and natural convection, the charge diffusion around the sphere is assumed to be Fickian:

$$\frac{\partial \Gamma_A}{\partial t} = D\nabla^2 \Gamma_A \qquad \textit{Equation 8}$$

$$where\ \nabla^2 = \left(\frac{\partial^2}{\partial r^2} + \frac{2\partial}{r\partial r} + \frac{1}{r^2}\frac{\partial^2}{\partial \theta^2} + \frac{cos\theta}{r^2 sin\theta}\frac{\partial}{\partial \theta} + \frac{1}{r^2 sin^2\theta}\frac{\partial^2}{\partial \varphi^2}\right)$$

Due to the symmetry of the model, the diffusion equation to be solved is independent of r and φ. Equation 8 reduces to

$$\frac{\partial \Gamma_A}{\partial t} = \frac{D}{r^2}\left(\frac{\partial^2 \Gamma_A}{\partial \theta^2} + \frac{1}{tan\theta}\frac{\partial \Gamma_A}{\partial \theta}\right) \qquad \textit{Equation 9}$$

At the start of the simulation, only species A is present and has a maximum coverage

$$t = 0 \; and \; \theta_{contact} < \theta < \pi; \begin{cases} \Gamma_A = \Gamma_A^* \\ \Gamma_B = 0 \end{cases} \qquad Equation\ 10$$

where t is time (s), Γ_A^* is the initial coverage of A and Γ_B is the surface coverage of species B (mol m^{-2}). Note $\Gamma_A + \Gamma_B = \Gamma_A^*$. From t = 0, a sufficient over-potential is applied at the electrode to fully drive the oxidation of A(ads) to B(ads) at the particle-electrode interface ($\theta = \theta_{contact}$)

$$t > 0 \; \begin{cases} D\left(\frac{\partial \Gamma_A}{\partial \theta}\right)_{\theta_{contact}} = -D\left(\frac{\partial \Gamma_B}{\partial \theta}\right)_{\theta_{contact}} \\ \Gamma_A|_{\theta_{contact}} = 0 \end{cases} \qquad Equation\ 11$$

The spherical particle is non-conductive and electrochemically inert. The net flux at the top of the sphere ($\theta = \pi$) is zero due to symmetry

$$D\left(\frac{\partial \Gamma_A}{\partial \theta}\right)\Big|_{\theta=\pi} = 0$$

Next, by using dimensionless parameters, the simulation model is generalised for the broad range of experimental parameters. The normalization of the dimensioned parameters is discussed in the next section.

2.2 Dimensionless parameters

The advantage of using dimensionless parameters for simulation as opposed to dimensional parameters is that first, the number of independent parameters is reduced to a minimum.[28] Consequently, second, the number of simulations required to describe a wide range of experimental conditions is reduced. The definition and normalization of the dimensionless parameters are shown in Table 1.

Table 1. Definition of dimensionless parameters. r_e is the radius of the inert sphere.

Dimensionless parameters		Normalisation
T	time	$\mathrm{D}t/{r_e}^2$
β_j	fractional surface coverage of species j	Γ_j/Γ_A^*
J	flux	$\frac{I}{FD\Gamma_A^*}$

The diffusion equation can be expressed in its dimensionless equivalent:

$$\frac{\partial \beta_A}{\partial T} = \frac{\partial^2 \beta_A}{\partial \theta^2} + \frac{1}{tan\theta}\frac{\partial \beta_A}{\partial \theta} \qquad \textit{Equation 12}$$

The boundary conditions become:

$$\left(\frac{\partial \beta_A}{\partial \theta}\right)_{\theta_{contact}} = -\left(\frac{\partial \beta_B}{\partial \theta}\right)_{\theta_{contact}} \qquad \textit{Equation 13}$$

$$T = 0,\ \ \theta > \theta_{contact} \begin{cases} \beta_A = 1 \\ \beta_B = 0 \end{cases} \qquad \textit{Equation 14}$$

$$T > 0 \begin{cases} \theta = \theta_{contact}, & \beta_A = 0 \\ \theta = \pi, & \frac{\partial \beta_A}{\partial \theta} = 0 \end{cases} \qquad \textit{Equation 15}$$

The dimensionless flux, J, can be calculated by the interfacial flux *or* the sum of the rate of change of material over the sphere surface:

$$J = 2\pi sin(\theta_{contact}) \left(\frac{\partial \beta_A}{\partial \theta}\right)\Big|_{\theta_{contact}} = -2\pi \int_{\theta_{contact}}^{\pi} \frac{\partial \beta_A}{\partial \tau} sin\theta d\theta \qquad \textit{Equation 16}$$

The next section will discuss the finite difference method used to solve the partial differential equation and boundary conditions outlined above.

2.3 Numerical simulation, convergence testing and validation

The partial differential equation for this one-dimensional system was discretised using the backward implicit method[28-29] with an expanding grid[30-31] in both the temporal (T) and spatial (θ) domains. The spatial grid expands exponentially from $\theta_{contact}$ to a maximum of π radians.

$$for\ \theta_{contact} < \theta < \pi: \qquad \theta_i = \theta_{i-1} + \Delta\theta\omega_\theta{}^i \qquad Equation\ 17$$

where $\Delta\theta$ is the initial spatial step, ω_θ is the spatial expansion factor and i is the step number. The temporal grid was discretised from zero with n small increments of ΔT before expanding exponentially to T_{max}.

$$T_k = T_{k-1} + \Delta T\omega_T{}^{k-n} \qquad Equation\ 18$$

where ΔT is the initial temporal step, ω_T is the temporal expansion factor (typically between 1 - 1.05) and k is the time step. The sets of discretised simultaneous equations subject to the outline boundary conditions were solved using the Thomas algorithm, using a LU matrix decomposition method.[28, 32]

The values of the spatial and temporal increments and their respective expansion factors (ω_θ and ω_T), were set to a small value to ensure numerical convergence and mass conservation. Mass conservation was constantly monitored throughout the simulation by comparing the flux at the interface and the rate of material depletion over the surface of the sphere; both expressions are shown in Equation 16 in the dimensionless form. The simulations were written and developed by the first author in Python *and* independently checked by a co-author (MY) in C++ with excellent agreement between the simulated results. The simulations were run on a dual Intel (R) Core (TM) E5-2640 v4 CPU 2.40 GHz PC with 16.00 GB of RAM, with a typical run time of less than 20 seconds.

3. Results and Discussion

This section reports the results of simulating diffusion over the surface of spheres and truncated spheres and characterisation using the diffusion indicator. Two notable features are expected as diffusion occurs across the surface of the sphere with various contact angles. First, for a small contact angle, the diffusion regime is expected to change as the 2-D Fickian diffusion occurs across the sphere surface to the 'sink' at the point-of-contact at $\theta = \theta_{contact}$. Possible regimes are: divergent diffusion of species B as surface expands with θ for when θ is less than $\pi/2$, Cottrellian behaviour when θ approaches $\pi/2$ and convergent diffusion of B as the available surface area 'shrinks' as θ increases beyond $\pi/2$. Species A and B show complementary behaviour and the description given relates to species B. These effects are illuminated and disentangled by the deployment of diffusion indicator, α. Second, in the long time limit, due to the finite amount of material on the surface of the sphere, the total available material diminishes and a 'thin-layer' response is expected. For the latter reason, initially, the diffusion indicator is first deployed to investigate the 'thin-layer' effect within a simple one-dimensional linear space so as to identify the thin layer fingerprint of the diffusion indicator.

3.1 Diffusion indication for thin-layer diffusional behaviour

The diffusion indicator, α, originally proposed by Haonan *et al.*,[23] distinguishes different diffusion regimes in simple electrode geometries. In his original work, semi-infinite diffusional transport to various electrode geometries was explored and the value of α was seen to transit and take values between 0 to 1 following a potential step in which the electrode is switched on at a certain time. The question arises as to what is the diffusion indicator fingerprint for a thin-layer diffusion regime? To answer

this, a simple one-dimensional simulation model in the Cartesian X-coordinate was first investigated considering *solution* phase diffusion.

Figure 2 a) shows a schematic of a one-dimensional model with boundary conditions corresponding to a potential step from a potential of zero current flow to a diffusion limited case. Herein, initially, species A is uniform in solution and the electrode at $x = 0$ is switched-on at $t = 0$ and act as a 'sink' of A:

$$Electrochemical\ reaction: A(aq) - e^- \rightarrow B(aq) \qquad Equation\ 19$$

The Fickian diffusion in one-dimension is

$$\frac{\partial c_A}{\partial t} = D_A \frac{\partial^2 c_A}{\partial x^2} \qquad Equation\ 20$$

where D_A is the diffusion coefficient of species A(aq), c_A is the concentration of A(aq) (mol m^{-3}) and x is the distance from the electrode interface (m). For thin-layer diffusion, A is constrained within the range $0 \leq x \leq l$ where l is the thin-layer thickness. Equation 20 can be converted into its dimensionless equivalent by using the following normalisation for time t, distance x and c_A:

$$T = \frac{D_A t}{l^2}, \quad X = \frac{x}{l} \quad and \quad C_A = \frac{c_A}{c_{A,bulk}} \qquad Equation\ 21$$

where $c_{A,bulk}$ is the bulk concentration of A(aq). The diffusion equation becomes:

$$Fickian\ diffusion: \quad \frac{\partial C_A}{\partial T} = \frac{\partial^2 C_A}{\partial X^2} \qquad Equation\ 22$$

To investigate the effect of thin-layer geometry, the outer spatial boundary of the simulation, $X = 1$, is set to a net of zero flux. The boundary conditions are thus:

$$Boundary\ conditions \begin{cases} T = 0,\ C_{A,\ 0 \leq X \leq 1} = C_{A,bulk} \\ 0 < T < T_{max},\ C_{A,X=0} = 0\ and\ \left(\frac{\partial C_A}{\partial X}\right)_{X=1} = 0 \end{cases}$$

$$Equation\ 23$$

where $T_{\max}$ is the duration of the potential step and is set to 100. $T \ll 1$ represents diffusion from a "semi-infinite" solution $\left(l \gg \sqrt{D_A t}\right)$ and $T \gg 1$ represents diffusion under thin-layer geometry $\left(l \ll \sqrt{D_A t}\right)$, respectively. Other modelling in one-dimension is reported in detail elsewhere.[28, 33-34]

Figure 2 b) shows a plot of diffusion indicator α against time T. Initially, Cottrellian diffusion ($\alpha = 0$) was seen. However, as T increases α was seen to deviate negatively from the Cottrellian limit. This is because A(aq) is depleted over all space for the duration of the simulation. Qualitatively the negative deviation of α is consistent with a smaller interfacial flux J as expected in the case of a thin-layer, in comparison to that for diffusion from a semi-infinite solution. Therefore the gradient of the log(J) with log(T) is smaller.

Quantitatively, the negative deviation of α from zero can be derived analytically for a thin-layer cell geometry. The flux-time relationship for a thin-layer cell with a limiting spatial extent of l can be solved analytically[35]:

$$J \propto \sum_{m=1}^{\infty} exp\left[\frac{-(2m-1)^2\pi^2 T}{4}\right] \qquad \textit{Equation 24}$$

The dotted green line overlaid in Figure 2 b) is the predicted α using the above analytical expression, with a summation up to $m = 7$ following substitution with equation 1. Excellent agreement is seen with the simulation result. In the long-time limit, the terms involving $m > 1$ in Equation 24 are approximately zero and the derivative of the logarithmic J with respect to time T can be approximated by $m = 1$:

$$\frac{\partial log(J)}{\partial T} \approx \frac{-\pi^2}{4} \qquad \textit{Equation 25}$$

Utilizing the fact that the differential of log(T) with respect to T is

$$\frac{dlog(T)}{dT} = \frac{1}{T} \qquad \textit{Equation 26}$$

substituting dT into Equation 25, and further into Equation 1, returns an expression of diffusion indicator α in the case of a thin-layer geometry:

$$\alpha = \frac{-\pi^2}{2} T + 1 \qquad \textit{Equation 27}$$

It is clear from Equation 27 that, the value of α is negative for large values of T.

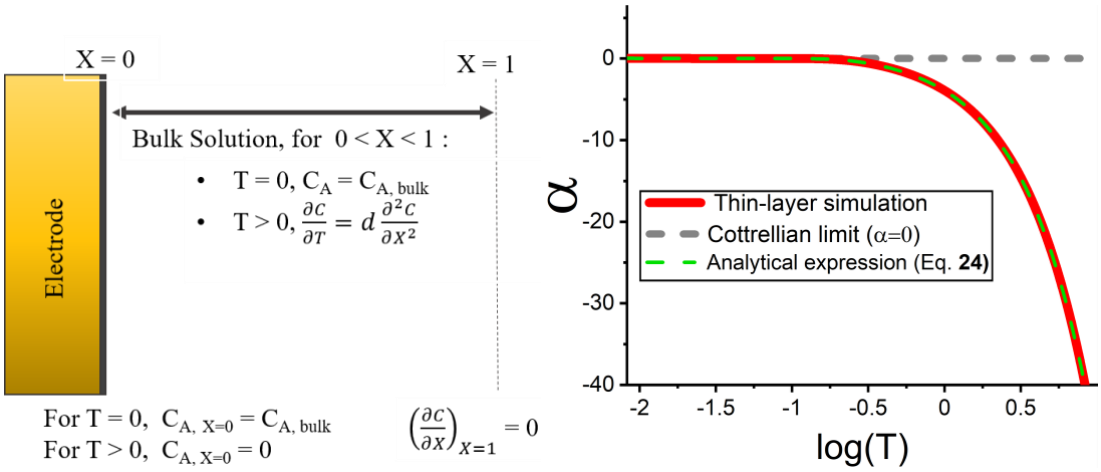

Figure 2 ***a****) Outline of the simple 1-D model in the Cartesian X coordinates. Species A is perturbed from the bulk concentration* $C_{A,\ bulk}$ *at the electrode interface (X=0) from time T=0.* ***b****) A plot of the diffusion indicator* α *against T. Simulation parameters:* T_{max} *= 100,* $\Delta X = 1x10^{-5}$, $\Delta T = 1x10^{-10}$, $\omega_{X,T} = 1.02$. *Overlaid as dotted line is the values obtained from Equation 24 with m = 7.*

Having understood the diffusion indicator for a thin-layer system where α tends to negative infinity in the long-time limit, we next return and investigate the flux-time transient for diffusion over the surface of a sphere.

Diffusion over the surface of a sphere

The diffusion over the surface of a sphere model in the dimensionless form is normalised to the radius of the sphere, diffusion coefficient and the initial coverage of A(ads), as outlined in the Theory section. Therefore, the only independent dimensionless variable in the simulation is the contact angle ($\theta_{contact}$), the effect of which is reported below.

Figure 3 shows the flux-time transients obtained from the simulation model for a wide range of $\theta_{contact}$ plotted in log-log form. At short times the initial interfacial flux J was seen to increase with the size of the contact angle, $\theta_{contact}$ corresponding to an increased injection of charge from the greater contact length. In general, as time progresses the flux was seen to decrease approximately linearly with time on the logarithmic scale for all contact angles before a sharp drop in flux was seen around log(T) = 0. The sharp 'fall-off' in the flux is seen to occur at a shorter times for larger $\theta_{contact}$. This is because of the finite amount of A(ads) initially adsorbed on the surface of the sphere and the total amount available for diffusion decreases as $\theta_{contact}$ increases.

From the flux-time transients it is unclear which diffusion regimes are in operation at different parts on the transient. Accordingly, next, the diffusion indicator, α, was deployed to illuminate the transition of diffusion regimes as a function of time.

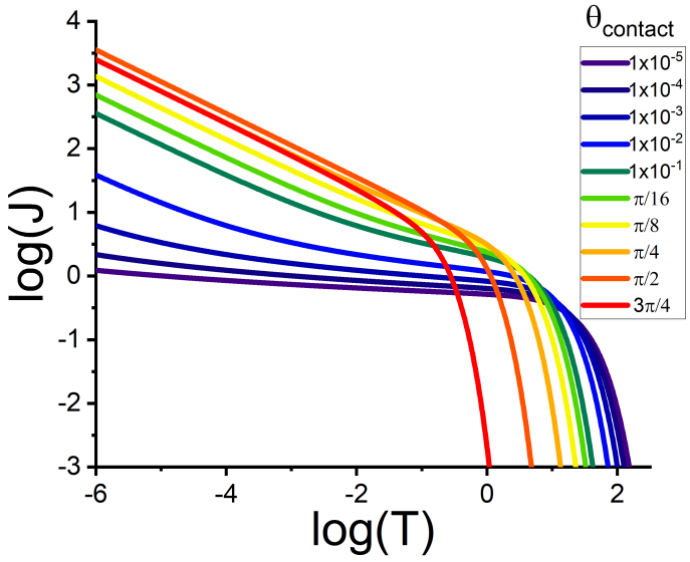

Figure 3. Dimensionless flux-time transient for diffusion over the surface of a sphere with various contact angles. From T = 0, an over-potential is applied at the electrode such that $\beta_{A,\theta_{contact}}$ equals zero. Other simulation parameters: $\Delta\theta = 1x10^{-8}, \Delta T = 1x10^{-10}, \omega_{\theta,T} = 1.02$ and $n = 1000$.

Figure 4 shows the diffusion indicator α values plotted against $\log(T)$ for the flux-time transients as seen in Figure 3. Overlaid (dotted lines) are the Cottrellian ($\alpha = 0$) and steady-state diffusion ($\alpha = 1$) limits, respectively.

For a very small contact angle $\theta_{contact}$ equal to $1x10^{-3}$, the diffusion indicator α transits from zero (Cottrellian) to near one, before it turns to negative values as time increases. In the short time limit, a Cottrellian response $(\alpha = 0)$ is expected because the diffusional distance is short relative to the size of the planar sink. As the diffusion occurs beyond the point(s) of contact, the sphere area is divergent (for the diffusion of B) up to angle $\theta = \pi/2$ leading to an 'enhancement' of mass transport to the planar sink, resulting in a quasi-steady-state flux, as indicated by $\alpha > 0$. At longer times, as material diffusion to and from beyond $\theta > \pi/2$, where the sphere surface area is convergent (for B), the amount of A available for diffusion diminishes resulting in a thin-layer effect as α tends towards negative infinity.

Of physical relevance, the smallest possible point-of-contact between a sphere to a plane is arguably a single atom and for a micron-sized sphere the corrosponding contact angle is approximately $1x10^{-5}$. One can see from Figure 4 that for this value α approaches to approximately 0.9. In the limit of a small $\theta_{contact}$, the two-dimensional surface diffusion to the small point of contact with a circumference underpinned by $\theta_{contact}$ might be crudely approximated by diffusion to an infinitely long cylinder electrode.[35] In this case the observation is fully consistent with the work by Haonan *et al.* where α was shown to approach ~0.9 in the case of Fickian diffusion to an infinitely long cylindrical electrode.[23]

For contact angles corresponding to a hemisphere $(\theta_{contact} = \pi/2)$ and beyond $(\theta_{contact} > \pi/2)$, the diffusion regime was initially Cottrellian ($\alpha = 0$) before a sharp

turn in the diffusion indicator to negative values ($\alpha < 0$) are seen as evident in Figure 4. The latter drop as characterised above, is due to the thin-layer effect. Notice that for these contact angle, α did not rise above zero at any time during the transient because truncated spheres ($\theta_{contact} \geq \pi/2$) do not contain divergent area regimes.

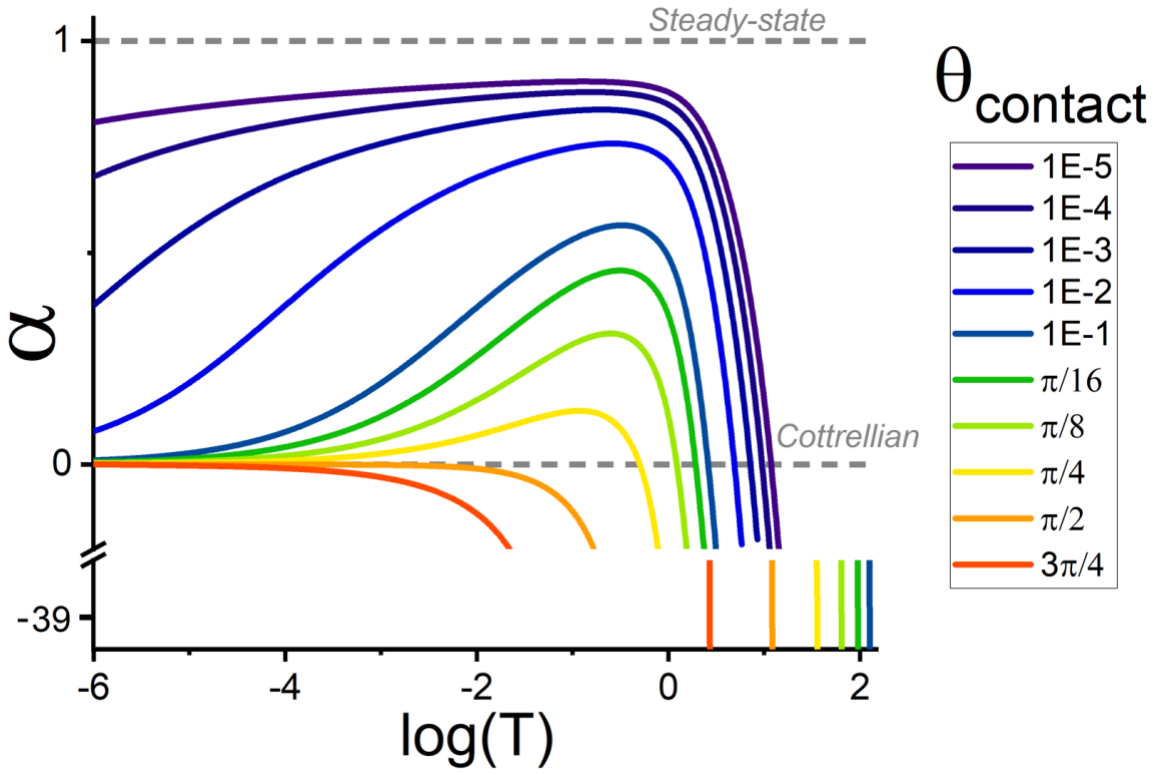

Figure 4. A plot of diffusion indicator, α, versus log(T) of the flux-time transients shown in Figure 3 a).

Figure 5 a) presents a plot showing the diffusion indicator α plotted against the percentage of the amount of A consumed during the charge injection. Interestingly for $\theta_{contact} = 1x10^{-5}$, for less than 1% of total consumption α has reached a quasi-steady-state value of 0.9 and then as $\theta_{contact}$ increases α was seen to gradually peak at values smaller than 0.9. Further interest emerges from Figure 5 b) which shows the surface coverage profile when 25% of the initial total materials have been consumed for the various $\theta_{contact}$. Three-dimensional surface plots are shown in Figure 5 c) for three different values of $\theta_{contact}, 1x10^{-5}, \pi/4 \; and \; \pi/2$. For the small $\theta_{contact}$ of

$1x10^{-5}$, the time required to consume 25% of the initial material is longer compared to the larger $\theta_{contact}$ because the total amount (mols) of A(ads) is proportional to the surface area of the sphere. Therefore, diffusion occurs over the entire surface of the sphere resulting in a near-uniform coverage, shown in Figure 5c). In contrast, for $\theta_{contact} = \pi/2$, the diffusion layer remained close to the particle-electrode interface when 25% of the starting material was consumed.

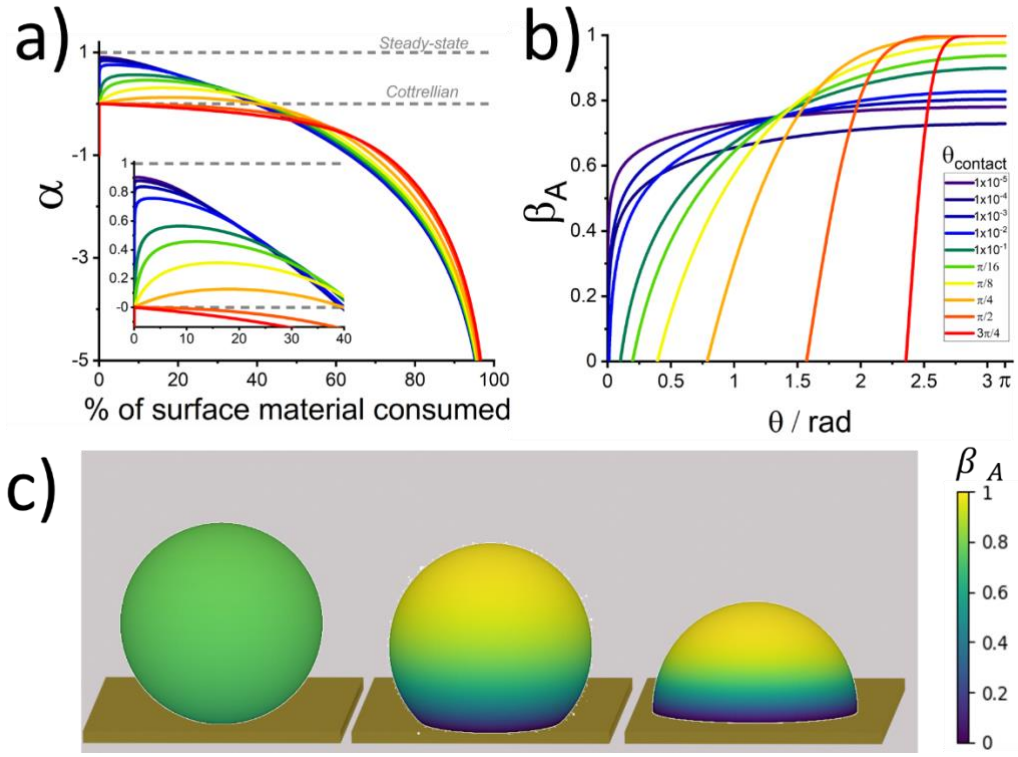

Figure 5. ***a****). A plot of the diffusion indicator, α, for the flux-time transients shown in Figure 3 a) vesus the percentage of materials consumed.* ***b****). Surface coverage profiles when 25% of materials are consumed for various $\theta_{contact}$. The colour coding is common to both a) and b).* ***c****) 3D visual representation of the surface coverage when 25% of the initial material has been consumed for three different contact angles. Left: $\theta_{contact}$ = 1x10^{-5}, centre: $\theta_{contact}$ = π/4, right: $\theta_{contact}$ = π/2.*

The results presented in dimensionless form herein are only dependent on the value of $\theta_{contact}$. Therefore, the simulated flux-time transients, the temporal evolution of α and the surface coverage profiles apply to all Fickian diffusion processes across the surface of a (truncated) sphere.

Conclusions

The diffusion indicator α was deployed to illuminate the transition between diffusion regimes as diffusion occurs over the surface of a sphere. For small contact angles, a Cottrellian behaviour was seen near the point-of-contact ($\alpha = 0$) to divergent as α approaches to 0.9 to convergent and eventually thin-layer as the material are depleted over the surface of the sphere ($\alpha \to -\infty$). The temporal evolution of α is indicative of the degree of sphere truncation. In the case of a thin layer, the diffusion indicator α was shown to scale negatively with T, excellent agreement was seen between analytical expression and simulation results.

Acknowledgements and Funding

This research did not receive any specific grant from funding agencies in the public, commercial, or not-for-profit sectors.

References

1. Heyrovsky, M.; Jirkovsky, J., Polarography and Voltammetry of Ultrasmall Colloids: Introduction to a New Field. *Langmuir* **1995**, *11*, 4288-4292.
2. Heyrovsky, M.; Jirkovsky, J.; Struplova-Bartackova, M., Polarography and Voltammetry of Aqueous Colloidal Tio2 Solutions. *Langmuir* **1995**, *11*, 4300-4308.
3. Heyrovsky, M.; Jirkovsky, J.; Struplova-Bartackova, M., Polarography and Voltammetry of Mixed Titanium (Iv) Oxide/Iron (Iii) Oxide Colloids. *Langmuir* **1995**, *11*, 4309-4312.
4. Dahneke, B., Particles and Photography. *Particulate Science and Technology* **1987**, *5*, 1-12.
5. Hailstone, R.; Liebert, N.; Levy, M.; McCleary, R.; Girolmo, S., Achieving High Quantum Sensitivities with Hydrogen Hypersensitization. I: Measurement. *Journal of imaging science* **1988**, *32*, 113-124.
6. Sokolov, S. V.; Eloul, S.; Kätelhön, E.; Batchelor-McAuley, C.; Compton, R. G., Electrode–Particle Impacts: A Users Guide. *Physical Chemistry Chemical Physics* **2017**, *19*, 28-43.
7. Rees, N. V., Electrochemical Insight from Nanoparticle Collisions with Electrodes: A Mini-Review. *Electrochemistry Communications* **2014**, *43*, 83-86.
8. Stevenson, K. J.; Tschulik, K., A Materials Driven Approach for Understanding Single Entity Nano Impact Electrochemistry. *Current Opinion in Electrochemistry* **2017**, *6*, 38-45.
9. Zhou, Y. G.; Rees, N. V.; Compton, R. G., The Electrochemical Detection and Characterization of Silver Nanoparticles in Aqueous Solution. *Angewandte Chemie International Edition* **2011**, *50*, 4219-4221.
10. Xu, W.; Zou, G.; Hou, H.; Ji, X., Single Particle Electrochemistry of Collision. *Small* **2019**, *15*, 1804908.

11. Bard, A. J.; Zhou, H.; Kwon, S. J., Electrochemistry of Single Nanoparticles Via Electrocatalytic Amplification. *Israel Journal of Chemistry* **2010**, *50*, 267-276.
12. Xie, R.-C.; Volokhova, M.; Boldin, A.; Seinberg, L.; Tsujimoto, M.; Yang, M.; Rasche, B.; Compton, R. G., Electrocatalytic Oxidation of Hydroxide Ions by Co3o4 and Co3o4@ Sio2 Nanoparticles Both at Particle Ensembles and at the Single Particle Level. *ChemElectroChem* **2020**, *7*, 1261-1276.
13. Yu, W.; Batchelor-McAuley, C.; Chang, X.; Young, N. P.; Compton, R. G., Porosity Controls the Catalytic Activity of Platinum Nanoparticles. *Physical Chemistry Chemical Physics* **2019**, *21*, 20415-20421.
14. Kuss, S.; Tanner, E.; Ordovas-Montanes, M.; Compton, R., Electrochemical Recognition and Quantification of Cytochrome C Expression in Bacillus Subtilis and Aerobe/Anaerobe Escherichia Coli Using N, N, N′, N′-Tetramethyl-Para-Phenylene-Diamine (Tmpd). *Chemical Science* **2017**, *8*, 7682-7688.
15. Sepunaru, L.; Tschulik, K.; Batchelor-McAuley, C.; Gavish, R.; Compton, R. G., Electrochemical Detection of Single E. Coli Bacteria Labeled with Silver Nanoparticles. *Biomaterials Science* **2015**, *3*, 816-820.
16. Sepunaru, L.; Plowman, B. J.; Sokolov, S. V.; Young, N. P.; Compton, R. G., Rapid Electrochemical Detection of Single Influenza Viruses Tagged with Silver Nanoparticles. *Chemical science* **2016**, *7*, 3892-3899.
17. Lin, C.; Kätelhön, E.; Sepunaru, L.; Compton, R. G., Understanding Single Enzyme Activity Via the Nano-Impact Technique. *Chemical Science* **2017**, *8*, 6423-6432.
18. Lin, C.; Sepunaru, L.; Kätelhön, E.; Compton, R. G., Electrochemistry of Single Enzymes: Fluctuations of Catalase Activities. *The Journal of Physical Chemistry Letters* **2018**, *9*, 2814-2817.
19. Chen, L.; Li, X.; Tanner, E. E.; Compton, R. G., Catechol Adsorption on Graphene Nanoplatelets: Isotherm, Flat to Vertical Phase Transition and Desorption Kinetics. *Chemical Science* **2017**, *8*, 4771-4778.
20. Lin, Q.; Compton, R. G., Quantifying Adsorption on Single Alumina Particles Via Impact Voltammetry and Current Transient Analysis. *The Journal of Physical Chemistry C* **2015**, *119*, 23463-23469.
21. Lin, Q.; Compton, R. G., Impacts Reveal and Quantify Monolayer Adsorption on Single Alumina Particles. *Russian Journal of Electrochemistry* **2017**, *53*, 994-1002.
22. Amatore, C.; Bouret, Y.; Maisonhaute, E.; Goldsmith, J. I.; Abruña, H. D., Ultrafast Voltammetry of Adsorbed Redox Active Dendrimers with Nanometric Resolution: An Electrochemical Microtome. *ChemPhysChem* **2001**, *2*, 130-134.
23. Le, H.; Kätelhön, E.; Compton, R. G., Characterising the Nature of Diffusion Via a New Indicator: Microcylinder and Microring Electrodes. *Journal of Electroanalytical Chemistry* **2019**, *855*, 113602.
24. Cottrell, F., Application of the Cottrell Equation to Chronoamperometry. *Z Physik Chem* **1902**, *42*, 385.
25. Le, H.; Compton, R. G., Comparative Chronoamperometry: Spheres, Discs, Cylinders and Bands. *Journal of Electroanalytical Chemistry* **2020**, *866*, 114149.
26. Murray, R. W., Chemically Modified Electrodes for Electrocatalysis. *Philosophical Transactions of the Royal Society of London. Series A, Mathematical and Physical Sciences* **1981**, *302*, 253-265.
27. Amatore, C.; Bouret, Y.; Maisonhaute, E.; Goldsmith, J. I.; Abruña, H. D., Precise Adjustment of Nanometric ‐Scale Diffusion Layers within a Redox Dendrimer Molecule by Ultrafast Cyclic Voltammetry: An Electrochemical Nanometric Microtome. *Chemistry ‐A European Journal* **2001**, *7*, 2206-2226.
28. Compton, R. G.; Katelhon, E.; Ward, K. R.; Laborda, E., *Understanding Voltammetry: Simulation of Electrode Processes*; World Scientific, 2020.
29. Euler, L., *Institutionum Calculi Integralis*, 1768; Vol. 1.
30. Gavaghan, D., An Exponentially Expanding Mesh Ideally Suited to the Fast and Efficient Simulation of Diffusion Processes at Microdisc Electrodes. 1. Derivation of the Mesh. *Journal of Electroanalytical Chemistry* **1998**, *456*, 1-12.

31. Gavaghan, D., An Exponentially Expanding Mesh Ideally Suited to the Fast and Efficient Simulation of Diffusion Processes at Microdisc Electrodes. 2. Application to Chronoamperometry. *Journal of electroanalytical chemistry* **1998**, *456*, 13-23.
32. Thomas, L. H., Elliptic Problems in Linear Difference Equations over a Network. *Watson Sci. Comput. Lab. Rept.* **1949**.
33. Yang, M.; Compton, R. G., Adsorption Processes Coupled with Mass Transport at Macro-Electrodes: New Insights from Simulation. *Journal of Electroanalytical Chemistry* **2019**, *836*, 68-76.
34. Yang, M.; Compton, R. G., Voltammetry of Adsorbed Species: Nonideal Interactions Leading to Phase Transitions. *The Journal of Physical Chemistry C* **2020**, *124*, 18031-18044.
35. Bard, A. J.; Faulkner, L. R., Fundamentals and Applications. *Electrochemical Methods* **2001**, *2*, 580-632.